Journal Name

ARTICLE TYPE

Cite this: DOI: 10.1039/xxxxxxxxxx

†

Received Date
Accepted Date

DOI: 10.1039/xxxxxxxxxx

www.rsc.org/journalname

Mutual regulation causes co-entrainment between a synthetic oscillator and the bacterial cell cycle

Marta Dies,[a,b] Leticia Galera-Laporta,[a,b] and Jordi Garcia-Ojalvo[a]

The correct functioning of cells requires the orchestration of multiple cellular processes, many of which are inherently dynamical. The conditions under which these dynamical processes entrain each other remain unclear. Here we use synthetic biology to address this question in the case of concurrent cellular oscillations. Specifically, we study at the single-cell level the interaction between the cell division cycle and a robust synthetic gene oscillator in *Escherichia coli*. Our results suggest that cell division is able to partially entrain the synthetic oscillations under normal growth conditions, by driving the periodic replication of the genes involved in the oscillator. Coupling the synthetic oscillations back into the cell cycle via the expression of a key regulator of chromosome replication increases the synchronization between the two periodic processes. A simple computational model allows us to confirm this effect.

Introduction

Oscillations are widespread in living organisms. Notably, multiple oscillatory phenomena coexist within cells with a wide variety of periods, ranging from seconds to days[1]. It is still not well understood how these cellular oscillators coordinate with each other inside a living cell. A first example of the interaction between cellular cycles that has been extensively studied in recent years is the gating of the cell cycle by the circadian clock. Evidence of this effect has been found so far in cyanobacteria[2,3], zebrafish[4], plants[5], and mouse fibroblasts[6] and liver cells[7]. This driving action has been attributed to transcriptional control of key cell-cycle regulators, such as Wee1, by clock proteins, such as the CLOCK-BMAL1 complex in mammalian cells[7]. Mathematical modelling has shown that this molecular mechanism enables the *entrainment* of the mammalian cell cycle by the circadian clock[8] (i.e. the cell cycle adapts its frequency to that of the circadian clock, resulting in the appearance of a stable phase relation between the two self-sustained oscillators[9]).

It is also to be expected that gene copy number variations, or even reciprocal regulation[10], should enable active driving in the opposite direction, namely from the cell cycle to the circadian clock. The existence of mutual co-entrainment is however still under debate, with some authors pointing directly to purely unidirectional coupling from the circadian clock to the cell cycle[7], as discussed in the preceding paragraph, and others hinting at the existence of a bidirectional interaction[11]. In this paper, we compare the entrainment arising from unidirectional and bidirectional coupling between two cellular rhythms in *Escherichia coli*, by using a synthetic gene oscillator as a proxy for the circadian clock, and by studying the interaction between this oscillator and the cell cycle. We study first the effect that chromosome replication has on the synthetic clock, via the periodic modulation of the copy number of the clock components. Next we introduce an ectopic coupling from the synthetic oscillator to the cell cycle, by placing one of the main cell cycle regulators under the transcriptional control of the proteins involved in the synthetic oscillator. Our results show that unidirectional coupling leads at best to a partial coordination of the two cellular rhythms, as measured by the level of phase synchronization[12] between the oscillators. These results are not necessarily straightforward, specially given the different nature of our two oscillators. When coupling two intrinsically different oscillators, the efficiency of unidirectional driving depends in principle on which oscillator is the driver and which one is the receiver (as discussed above regarding the coupling between the circadian clock and the cell cycle), and may not be necessarily worse than for mutual coupling (specially when the intrinsic frequencies of the two oscillators are not close to each other). We show, however, that this is indeed the case: bidirectional coupling is needed in our case in order to cause a significant level of co-entrainment.

The bacterial cell cycle consists in cell growth, chromosomal replication, and cell division[13]. In general, for all bacterial species and during the exponential phase, this natural genetic os-

[a] *Dept. of Experimental and Health Sciences, Universitat Pompeu Fabra, Barcelona Biomedical Research Park, 08003 Barcelona, Spain. E-mail: jordi.g.ojalvo@upf.edu*
[b] *Dept. of Physics and Nuclear Engineering, Universitat Politècnica de Catalunya, 08222 Terrassa, Spain.*

cillator has a fairly constant period under a fixed set of conditions (such as temperature and culture medium). During bacterial duplication, it is critical to ensure that daughter cells will inherit one copy of the chromosome, and only one. Hence, chromosomal replication must occur only once per cell division. Replication in *E. coli* is initiated at a specific site of the DNA, known as *oriC*, where the replication machinery conformed by several proteins is recruited forming multimeric complexes. The formation of these complexes is triggered by specific proteins, such as DnaA[14,15]. Only the active form of DnaA initiates replication. Once the process has started, cell needs to inhibit DnaA activity to ensure that replication occurs only once per cell division. *E. coli* presents three main DnaA-regulatory mechanisms, one of them consisting in the so-called the regulatory inactivation of DnaA (RIDA) system. The RIDA system is essentially formed by the Hda protein and the beta subunit of DNA polymerase III holoenzyme, encoded by *dnaN* gene. This RIDA complex forms a sliding clamp on DNA that converts the active ATP-DnaA to the inactive ADP-DnaA form, thus preventing replication re-initiation[15–17]. One of the consequences of chromosomal replication is that across the cell cycle bacteria change the number of copies of the genome, and this change follows the periodicity of the cell cycle. In this way the cell cycle drives the number of proteins of transcribed genes[18], which leads to an unavoidable driving of all gene-based oscillators operating inside a cell.

As mentioned above, here we study how the cell cycle oscillations described above are coupled with a synthetic oscillator. Due to its robustness and controllability, we chose the tunable oscillator designed by Stricker et al in 2008[19]. This synthetic oscillator was engineered using the inducible combinatorial promoter $P_{lac/ara}$, whose transcription is activated by the AraC protein in the presence of arabinose, and repressed by the LacI protein in the absence of isopropyl β-D-1-thiogalactopyranoside (IPTG) (see Figure 1A). The two components of the oscillator (the *araC* and *lacI* genes) and the green fluorescent protein (*gfp*) gene that acts as a reporter, were marked with a degradation tag and were placed under the control of three identical copies of the $P_{lac/ara}$ promoter. These elements were then introduced into two different plasmids and transformed into a genetically modified *E. coli* strain with deletions in the *araC* and *lacI* wild-type genes, conforming the JS011 strain[19]. High enough AraC levels result in a higher transcription of the three elements (positive feedback), but once a critical level of LacI is reached the transcription is slowed down (negative feedback). The combined dynamics of these two feedback loops leads to oscillations in protein expression levels, as can be seen in Figure 2A below.

In order to couple the state of the synthetic oscillator to the cell cycle, we designed and constructed a plasmid (pMiL101) that contains a copy of the *hda* and *dnaN* genes (members of the RIDA system) under the control of the $P_{lac/ara}$ promoter. We subsequently introduced this plasmid into the synthetic oscillator strain JS011[19], conforming a bidirectionally coupled strain (see section "Experimental Methods" below for details). Figure 1B shows a diagram of the synthetic oscillator back-coupled to chromosomal replication. To ensure a fair comparison between the unidirectional and bidirectional coupling cases, we transformed

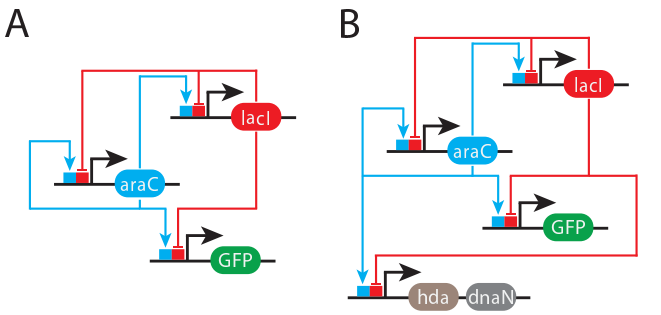

Fig. 1 Network diagrams of the synthetic oscillator and its coupling to chromosomal replication. (A) The hybrid promoter $P_{lac/ara}$ controls the transcription of *araC* and *lacI* genes, forming a positive and a negative feedback loop, respectively. *gfp* acts as a reporter of the state of the genetic oscillator. (B) Another copy of the hybrid promoter $P_{lac/ara}$ drives the transcription of the *hda* and *dnaN* genes, members of the RIDA system that inhibit the initiation of chromosomal replication.

the pMiL101 plasmid backbone (this is, the plasmid containing only the origin of replication and the antibiotic resistance, without the back-coupling to replication) into JS011 (see section "Experimental Methods" below). We will refer to this strain as the unidirectional strain.

Results

Effect of mutual coupling on the oscillator periods

We started by characterizing the synthetic oscillator driven by the cell cycle using the unidirectional strain. We filmed microcolonies of this strain with time-lapse fluorescence microscopy, and tracked individual cells while growing in a minimal medium containing 0.7 % (w/v) Arabinose and 2 mM IPTG (see section "Growth conditions for microscopy" for details on cell culture and imaging). Figure 2A shows a filmstrip of the unidirectional strain, with the GFP signal coloured in green. An heterogeneous "off-on-off-on" pattern in GFP fluorescence can be discerned in single cells, reflecting oscillations in the expression of the reporter. Time traces of cell length and fluorescence for three independent lineages are plotted in Figure 2B. Analysis of data shows that the mean cell cycle period is $\sim 47 \pm 12$ min and the mean period of the synthetic oscillator is $\sim 54 \pm 11$ min under our experimental conditions. The distributions of these two quantities are shown in Figure 3A.

Figure 2C shows the time traces of the synthetic oscillator back-coupled to chromosomal replication using the bidirectional strain. In this case, when AraC and LacI in the synthetic oscillator are expressed at a high level, the RIDA system is also overexpressed, thus inhibiting replication initiation. In these conditions the periods are $\sim 46 \pm 13$ min for the cell cycle and $\sim 54 \pm 10$ min for the synthetic oscillator under the same experimental conditions as the previous case. The corresponding distributions of the two quantities are shown in Figure 3B. Hence, introducing the back-coupling in the system seems not to affect the period distributions of any of the two oscillators. These distributions are also significantly different between the two oscillators, with the periods of the synthetic clock being in general larger than those of the cell cycle. We thus asked next if the two oscillators can mutually lock

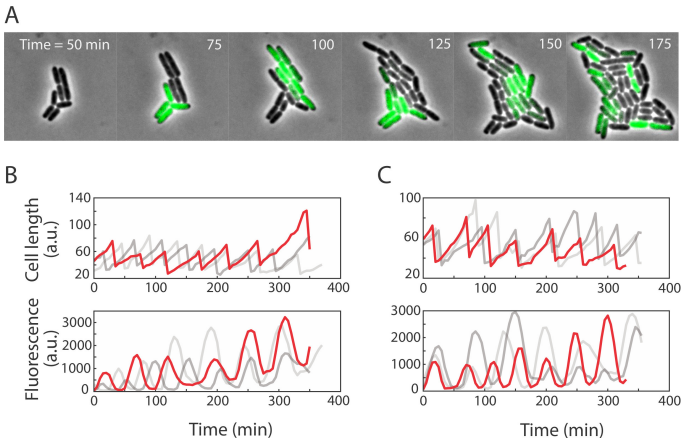

Fig. 2 Tracking the natural and synthetic oscillators. (A) Filmstrip of the unidirectional strain, in which the synthetic gene oscillator is modulated by periodic chromosome replication. GFP fluorescence (coloured in green) follows an heterogeneous "off-on-off-on" oscillating pattern in single cells. Panels (B) and (C) show cell length (top) and GFP fluorescence (bottom) time traces in independent lineages for the unidirectional case and the bidirectional one, respectively. The red line highlights one of the three lineages measured, for clarity.

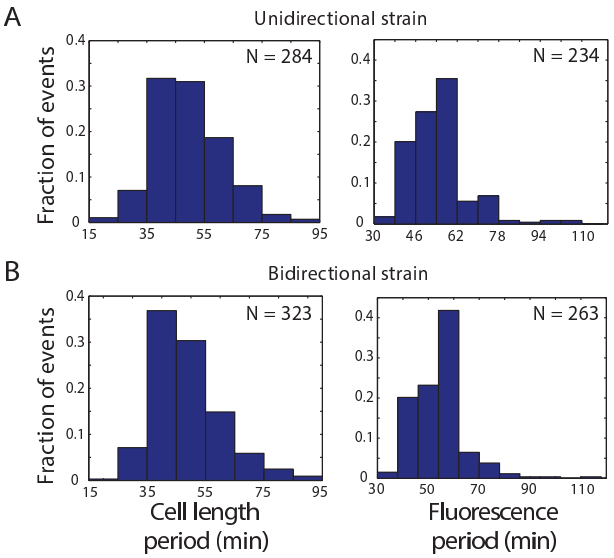

Fig. 3 Experimental distributions of the periods of the cell cycle (left) and synthetic (right) oscillators. (A) Unidirectional strain, fo which the mean value plus/minus standard deviation of the period is $\langle T_L \rangle = 47 \pm 12$ min for the cell cycle and $\langle T_F \rangle = 54 \pm 11$ min for the synthetic oscillator. (B) Bidirectional strain: $\langle T_L \rangle = 46 \pm 13$ min and $\langle T_F \rangle = 54 \pm 10$ min.

in phase in these conditions.

Effect of mutual coupling on the oscillator phases

Given that in the bidirectional strain, the synthetic oscillator controls the overexpression of the RIDA system, we are directly acting on the replication time. To determine the phase relationship between the two oscillators[9], we proceeded to define a phase that accounts for the progress of the system through a cycle, and correspondingly assigned it to each point of the time series data of the two oscillators. We defined a cycle as the segment of data going from one minimum of cell length to the following maximum (thus spanning the entire cell life), and fixed this phase to be 0 at the beginning of the cycle (when the cell is born) and 1 at the end of the cycle (just before the cell divides). As experimental data is sampled at a fixed interval, it is straightforward to assign the intermediate values for the phase assuming a linear progression along the cycle. Fluorescence data was also segmented according to cell length cycles, and phases were assigned correspondingly.

We are now prepared to quantify the existing phase shift between the two oscillators by asking when fluorescence maxima occur within a cell length cycle. The distributions of the timing of fluorescence maxima within a cell length cycle are shown in Figure 4 for the unidirectional strain (left panel) and for the bidirectional one (right panel). For the sake of clarity, phase has been redefined so that 0.5 corresponds to the moment when cell achieves its maximum length (right before division). The data shows that only in the bidirectional case the distribution of fluorescence maxima is clearly unimodal (and centred around the division time).

In order to measure the distances between these two distributions we used the Kullback-Leibler (KL) divergence. Briefly, we computed the KL distances of the subsampled distributions intra-groups (this is, between 100 subsamples of 50 values randomly chosen from the unidirectional strain phase shift data on the one hand, and between 100 subsamples of 50 randomly chosen values from the bidirectional strain phase shift data on the other) and we used these two distances as controls. Then we computed the KL distances of the subsampled distributions inter-groups (this is, between the subsamples of the unidirectional strain data and the subsamples of the bidirectional strain data). Finally, we compared the KL distances between the controls and the inter-group using a non-parametric test (Wilcoxon rank sum test). In the case of the unidirectional strain control distance versus inter-group distance, the test rejects the null hypothesis that the two sets of data come from distributions with equal median with p-value$= 2 \cdot 10^{-4}$. In the case of the bidirectional strain control distance versus inter-group distance the null hypothesis is rejected with p-value$= 0.02$. This statistical analysis implies that the histograms in Figure 4 are statistically different.

Taken together, our results suggest that the intrinsic driving of the synthetic oscillator by the cell cycle (via the modulation of the chromosome copy number) is not strong enough for the latter to entrain effectively the former (left panel of Figure 4). On the other hand, when we couple the synthetic clock back into the cell cycle the entrainment increases noticeably (right panel of Figure 4).

Computational model

In order to interpret the experimental results and verify whether entrainment increases due to back-coupling, we implemented a simple computational model. Since the unidirectional system (this is, the synthetic oscillator driven by the cell cycle) is a particular case of the more general scenario depicted by the bidirectional system (where the synthetic oscillator is back-coupled to

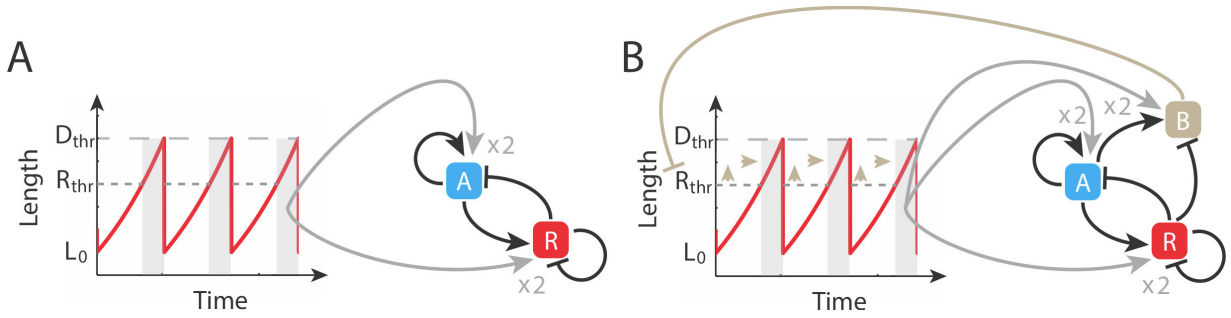

Fig. 5 Diagrams of model interactions. Cell length increases exponentially between division events. When it reaches the replication threshold (R_{thr}) all the productions from the synthetic oscillator are doubled (gray areas). Once cell length arrives to the division threshold (D_{thr}) it returns to its initial value (L_0) and the synthetic oscillator productions are reset to their original rates. This applies to both the unidirectional (A) and bidirectional (B) cases. In (B), the oscillator inhibits replication initiation by increasing R_{thr} so that it narrows the time intervals where oscillator production rates are doubled (gray areas are pushed towards the right).

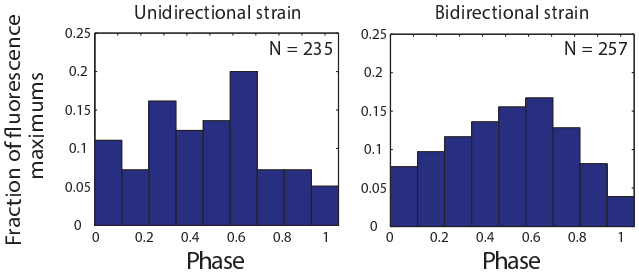

Fig. 4 Phase shift between the two oscillators. The distributions of the timing of fluorescence maxima within a cell length cycle are plotted for the unidirectional (left) and bidirectional (right) cases. The *x* axis covers one full cycle of cell division. For better visualization, the phase has been redefined so that a phase equal to 0.5 indicates the instant at which the cell length is maximal.

chromosomal replication), we will introduce first the bidirectionally coupled model and will explain the specificities of the unidirectional system as a particular case of the back-coupled model.

For the synthetic oscillator, we developed a reduced model based in an activator-repressor system[20] where only two species are described: the activator, A, and the repressor, R, both controlled by the same promoter. The dynamics of these two species is described by Equation (1)a-b (see section "Modelling the synthetic oscillator" for details). Besides, the influence of the synthetic oscillator on replication is modeled by considering the production of the RIDA system (B), which is also controlled by the hybrid promoter, $P_{lac/ara}$, as given by Equation (1)c.

In turn, the cell cycle was modelled as an integrate and fire mechanism, in which cell length grows exponentially (Equation (1)d) and two thresholds trigger chromosomal replication and cell division events. In this way, when cell length reaches the first threshold (replication, R_{thr}) the productions of all the synthetic oscillator elements are doubled (as the copy number of genes is increased by 2-fold) (Equation (2)). We are assuming here that all the considered species are transcribed at the same time (given that all the modelled genes are located in plasmids, the delays associated to replicating genes at different distances from the origin of replication are small). B is assumed to increase the threshold R_{thr}, in a way that mimics its inhibitory effect on replication (Equation (3)). Once the cell length arrives to the second threshold (division, D_{thr}), it returns to its initial value L_0 and the production rates are reset to their original values. The full model is:

$$\frac{dA}{dt} = \alpha_1\zeta + \frac{\beta_1\zeta A^n}{K^n + A^n + (\gamma R)^p} - \delta_1 A \tag{1a}$$

$$\frac{dR}{dt} = \alpha_2\zeta + \frac{\beta_2\zeta A^n}{K^n + A^n + (\gamma R)^p} - \delta_2 R \tag{1b}$$

$$\frac{dB}{dt} = \alpha_3\zeta + \frac{\beta_3\zeta A^n}{K^n + A^n + (\gamma R)^p} - \delta_3 B \tag{1c}$$

$$\frac{dL}{dt} = \alpha_0 L \tag{1d}$$

where $\alpha_0 = L_0/\tau$ (with τ being the characteristic time of cell cycle). ζ is a parameter that reflects the driving of the synthetic oscillator by chromosomal replication:

$$\zeta = \begin{cases} 1 & \text{for } L_0 \le L < R_{thr} \\ 2 & \text{for } R_{thr} \le L < D_{thr}\ , \end{cases} \tag{2}$$

As mentioned above, B mediates the coupling of the synthetic oscillator to the chromosomal replication, by increasing the replication threshold:

$$R_{thr} = D_{thr} \cdot \left(\varepsilon + \frac{\eta \cdot \kappa \cdot B}{B + K_l}\right) . \tag{3}$$

Here $\varepsilon \in (0,1)$ is the fraction of the division threshold at which replication occurs when the synthetic oscillator is not back-coupled to replication ($\eta = 0$). When back-coupling is introduced ($0 < \eta \le 1$) R_{thr} increases and approaches D_{thr}. As the term $B/(B+K_l)$ saturates to 1, the maximum limit where replication can happen (considering the strongest back-coupling, so $\eta = 1$) is $R_{thr} = D_{thr}(\varepsilon + \kappa)$. We chose $\kappa = 0.9 \cdot (1-\varepsilon)$ because it is not biologically realistic that replication occurs simultaneously to cell division.

Note that since all our exogenous genes are controlled by the same promoter ($P_{lac/ara}$), we consider the parameters K, n, p and γ to be the same for species A, R and B. Figure 5 shows two diagrams for the model interactions for the unidirectional and the bidirectional cases.

We introduced variability in the deterministic model described above by allowing random variation in the reaction rates among different cell cycles. To that end, for each cell cycle we drew parameter values randomly from a Gaussian distribution with mean values shown in Table 1 and standard deviations ranging from 2% of the mean value in the case of the synthetic oscillator parameters (Equation (1)a-c) up to 18% in the case of initial cell length L_0. These ranges were adjusted such that the statistical distributions of different oscillator features were in agreement with experimental results. In particular, as seen in Figure 6 the experimental distributions of the lengths of newborn cells (top row) have a width of ∼18% for both the unidirectional and the bidirectional strains. In turn, the division ratio (bottom row) has a width of 11%. Also, given that the maximum cell length distributions do not change (middle row), we assumed that back-coupling only affected the replication threshold (by incrementing its value and approaching it to the division threshold, as explained above) and we left the division threshold unchanged.

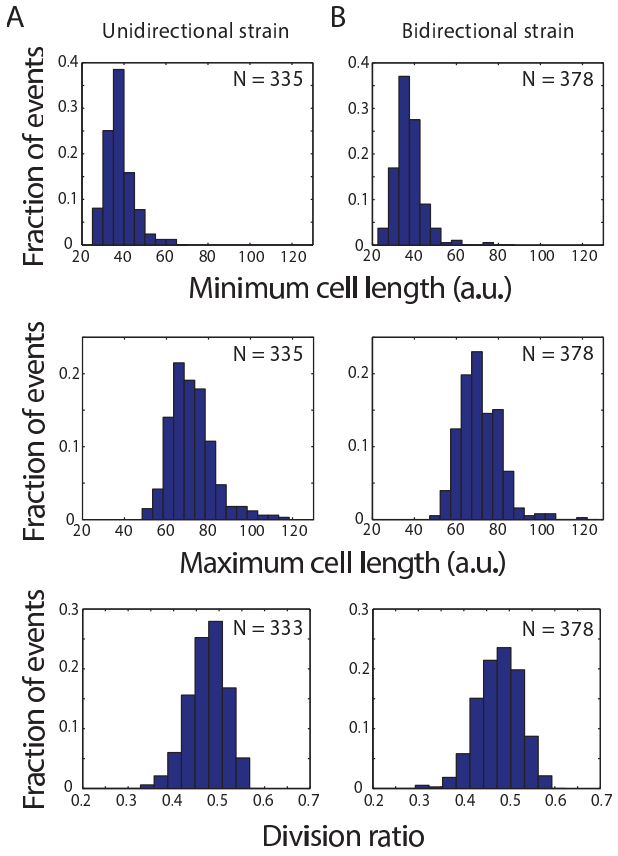

Fig. 6 Experimental distributions for the cell length minima, maxima and division ratio. (A) Unidirectional strain: newborn cell length distribution (upper panel), $\langle L_{min} \rangle = 38 \pm 7$ a.u, maximum cell length distribution (medium panel), $\langle L_{max} \rangle = 72 \pm 11$ a.u., and cell division ratio distribution (defined as $\rho = (L_{max} - L_{min})/L_{max}$, bottom panel), $\langle \rho \rangle = 0.47 \pm 0.05$. (B) The same distributions are plotted for the bidirectional strain: $\langle L_{min} \rangle = 37 \pm 7$ a.u, $\langle L_{max} \rangle = 71 \pm 10$ a.u., and $\langle \rho \rangle = 0.47 \pm 0.06$.

Mutual co-entrainment in the model

Figure 7 shows the time series for the synthetic oscillator driven by cell cycle ($\eta = 0$, left) and back-coupled to chromosomal replication ($\eta > 0$, right), corresponding to the experiments with the unidirectional and the bidirectional strains, respectively. To allow comparison, experimental time traces for these strains in one independent lineage are also plotted. We focused in the activator (A) expression to account for the synthetic oscillator state, as the model does not consider a fluorescent reporter. The replication threshold (R_{thr}) has been indicated in every cell cycle as a vertical gray bar. For $\eta = 0$ the periods obtained for the division and synthetic oscillators are $\langle T_L \rangle = 44 \pm 14$ min and $\langle T_A \rangle = 45 \pm 13$ min, respectively. For $\eta = 0.4$ the values obtained are $\langle T_L \rangle = 45 \pm 17$ min and $\langle T_A \rangle = 46 \pm 12$ min (see Figure 8). Hence, the mean values and deviations of the periods obtained in simulations are in agreement with the experimental ones.

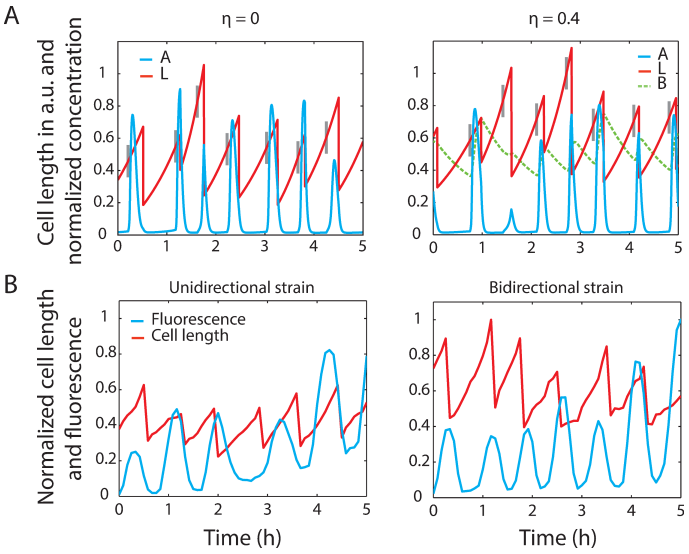

Fig. 7 Simulated and experimental time series of the coupled oscillators for the unidirectional (left) and bidirectional (right) cases. (A) Numerical integration of the coupled oscillator model. Cell length (L) is shown in red and the normalized concentration of the activator (A) in blue. In every cell cycle, the replication threshold (R_{thr}) is indicated as a vertical gray bar. In the bidirectional case (right) the time series for B is also plotted (green dashed line). (B) Experimental time traces of the cell length (red line) and GFP fluorescence (blue line) in one independent lineage for the unidirectional and the bidirectional strains. Data from Figure 2 (solid red lines in that Figure).

In order to quantify the phase shift between the cell cycle and the synthetic oscillator, we assigned a phase to the simulated time series in exactly the same way as we did for experimental data (see section "Effect of mutual coupling on the oscillator phases"). As a control, Figure 9 shows the theoretical case in which the synthetic oscillator is not driven by the bacterial cell cycle, nor back-coupled to replication. Panel B shows the histogram of the timing of activator concentration maxima within a cell length cycle. Again, phase has been redefined so that 0.5 indicates the instant when cell length is maximal.

The results for the unidirectional ($\eta = 0$) and the bidirectional ($\eta = 0.4$) cases are plotted in Figure 10, where the distributions of

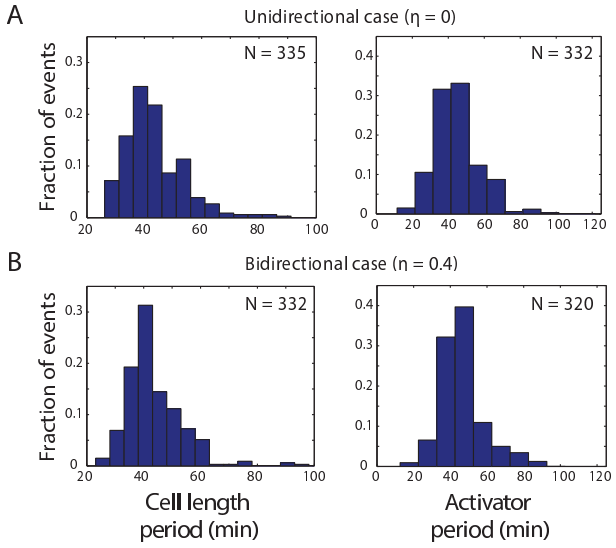

Fig. 8 Distributions of the periods of the cell cycle and synthetic oscillators obtained from the computational model. (A) Unidirectional case ($\eta = 0$), for which the mean values plus/minus standard deviation of the period were obtained for the cell cycle, $\langle T_L \rangle = 44 \pm 14$ min, and the synthetic oscillator, $\langle T_A \rangle = 45 \pm 13$ min. (B) Bidirectional case ($\eta = 0.4$), $\langle T_L \rangle = 45 \pm 17$ min and $\langle T_A \rangle = 46 \pm 12$ min.

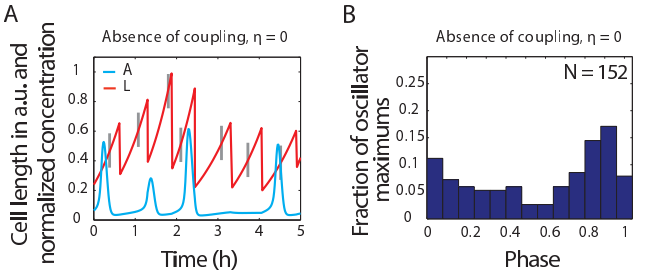

Fig. 9 Time series and phase shift between the synthetic and cell-cycle oscillators in the absence of coupling. We have considered the ideal case in which the synthetic oscillator is not driven by bacterial cell cycle, nor back-coupled to replication. (A) Time series for cell length (L), in red, and the normalized concentration of the activator (A), in blue, are plotted. In every cell cycle, the replication threshold (R_{thr}) is indicated as a vertical gray bar. The periods for the cell length and synthetic oscillators are $\langle T_L \rangle = 43 \pm 13$ min and $\langle T_A \rangle = 100 \pm 50$ min, respectively. (B) Histogram of the timing of activator concentration maxima within a cell length cycle. As in the section "Effect of mutual coupling on the oscillator phases", the phase has been redefined so that 0.5 corresponds to L being maximal.

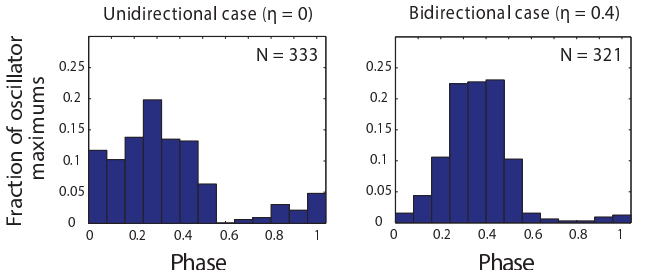

Fig. 10 Phase shift between the two simulated oscillators. Histograms of the timing of activator concentration maxima within a cell length cycle are plotted for the unidirectional ($\eta = 0$, left panel) and bidirectional ($\eta = 0.4$, right panel) cases. As in section "Effect of mutual coupling on the oscillator phases", the phase has been redefined so that 0.5 corresponds to a maximal cell length. These results are in agreement with the experimental ones (Figure 4).

the timing of activator concentration maxima within a cell length cycle are shown for each case. The computational results are in good qualitative agreement with experiments (quantitative agreement is precluded by model simplifications, such as the lack of dynamical noise). The results confirm that only the case of reciprocal coupling, $\eta = 0.4$, leads to a clear unimodal peaked distribution.

Comparing the histogram in Figure 9B with those in Figure 10 we can appreciate that in the case of mutual coupling the synthetic oscillator is noticeably entrained by the cell cycle, with respect to the control situation depicted in Figure 9. This confirms that mutual regulation effectively leads to co-entrainment of the cell cycle and our synthetic oscillator.

Conclusion

There are multiple ways by which biochemical circuits can be coupled inside cells, leading to substantial coordination of cellular processes[21]. A common coupling mechanism is via transcriptional regulation of a circuit component by a protein involved in a different circuit. This is the case, for instance, of the gating of the cell cycle by the circadian clock[7]. An intrinsic, passive mode of coupling occurs in principle between the cell cycle and gene-based circuits, since the expression levels of the circuit components oscillate periodically following the chromosome replication cycle of the cell. It is thus natural to ask whether this copy number modulation is enough to entrain gene oscillators to the cell cycle, or if some sort of back-coupling (in the form for instance of gene regulation, as mentioned above) is needed for effective entrainment to arise between the two rhythms.

Here we have used synthetic biology to address this question. Specifically, we have studied at the single-cell level the interaction between the bacterial cell cycle and a robust synthetic oscillator in *E. coli*. Our results show that cell replication and division are unable to strongly entrain the synthetic oscillations consistently under normal growth conditions, even though the genes involved in the oscillator are being replicated periodically. It is only when the synthetic oscillations are coupled back into the cell cycle via the expression of a key regulator of chromosome replication (the RIDA system), that the two periodic processes become significantly co-entrained. A simple computational model, constrained by the experimental observations in terms of the statistical properties of the oscillators, allows us to confirm this effect. Our results are potentially relevant for the design of robust synthetic oscillators, by showing that the inclusion of components that couple these oscillators with the chromosome replication machinery alters their natural behavior, by making them entrain to the cell division cycle.

Experimental methods

Plasmid and strain construction

The *E. coli* strain DH5α was used to clone all plasmids using standard molecular cloning techniques. Plasmid pMiL001 was con-

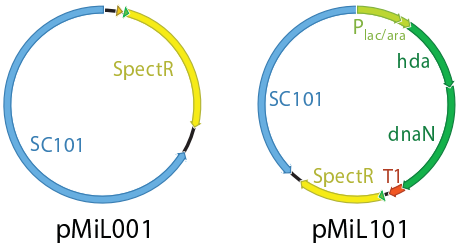

Fig. 11 Plasmids diagrams. Plasmid pMiL001 contains only the origin of replication (SC101) and the antibiotic resistance gene (spectinomycin). This plasmid was transformed into the synthetic oscillator "wild-type" strain (JS011) to conform the unidirectional strain. Plasmid pMiL101 contains the origin of replication (SC101), the antibiotic resistance gene (spectinomycin), and the construct $P_{lac/ara}$-*hda-dnaN-T1* (responsible for back-coupling the synthetic oscillator to chromosomal replication). This plasmid was transformed into JS011 to form the bidirectional strain.

structed *de novo* by assembling the origin of replication SC101 and the gene for spectinomycin resistance. Plasmid pMiL101 was constructed cloning the construct $P_{lac/ara}$-*hda-dnaN-T1* into pMiL001 (*T1* being the transcriptional terminator used in the synthetic oscillator) (see Figure 11). $P_{lac/ara}$ and *T1* fragments were amplified by PCR from the original synthetic oscillator strain (JS011). In turn, *hda* and *dnaN* genes were amplified from the wild-type *E. coli* MG1655 genome. Both plasmids were verified by sequencing.

The unidirectional strain was constructed transforming the plasmid pMiL001 into the original synthetic oscillator strain JS011 (kind gift from Prof. J. Hasty, University of California San Diego). The bidirectional strain was constructed transforming the plasmid pMiL101 into JS011.

Growth conditions for microscopy

Cells were grown overnight from glycerol stocks at 37°C in Luria Broth (Miller's modification) (LB) with appropriate antibiotics for selection (added to the following final concentrations: 100 μg/ml ampicilin, 50 μg/ml kanamycin, and 50 μg/ml spectinomycin), and then diluted back in LB with the corresponding antibiotics and inductors: 0.7% (w/v) arabinose and 2 mM IPTG, to a final $OD_{600} = 0.02$. This culture was grown at 37°C until $OD_{600} = 0.2$. After this, cells were diluted 1:5 in A minimal medium (composition per 100 ml: 20 ml A Salts (5x), 80 ml sterile deionized water, 100 μl $MgSO_4 \cdot 7\ H_2O$ (1 M), 250 μl Glycerol (80%), and 1 ml CasaAa (10%); A Salts (5x) composition per 100 ml: 0.046 g $(NH_4)_2SO_4$, 2.25 g KH_2PO_4, 5.25 g K_2HPO_4, 0.25 g sodium citrate tribasic $\cdot$ 2 H_2O, and 100 ml sterile deionized water[22]) with inductors and 0.4% (w/v) glucose. 50 μl of this diluted culture were spotted onto a low-melt agarose pad made of A minimal medium 2% (w/v) and containing the inductors and 0.4% (w/v) glucose. Cells were grown in the pad at 37°C for 2 h and then were vortexed in 10 ml of A minimal medium. 2.25 μl of the resulting "supernatant" were spotted onto a freshly prepared A minimal medium 2% (w/v) low melt agarose pad containing the inductors and 0.4% (w/v) glucose that was placed afterwards into a coverslip-bottom Willco dish for imaging.

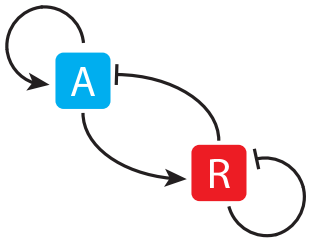

Fig. 12 Diagram of interactions for the synthetic oscillator reduced model. The activator (A) promotes its own production and the repressor (R) one. In turn, the repressor inhibits the expression of A and its own.

Theoretical methods

Modelling the synthetic oscillator

Stricker *et al.* proposed a detailed molecular model for their synthetic oscillator consisting in 73 reactions, 27 species and 27 parameters. The authors explicitly considered intermediate processes such as dimerization of AraC and tetramerization of LacI[19]. Due to the difficulty to work with such a complex model, we implemented a low-dimensional model based on minimal mechanisms, inspired by the model from Rue *et al.* Rué and Garcia-Ojalvo[20]:

$$\frac{dA}{dt} = \alpha_1 + \frac{\beta_1 A^n}{K^n + A^n + (\gamma R)^p} - \delta_1 A \tag{4a}$$

$$\frac{dR}{dt} = \alpha_2 + \frac{\beta_2 A^n}{K^n + A^n + (\gamma R)^p} - \delta_2 R \tag{4b}$$

Here A is the activator (AraC dimers) and R the repressor (LacI tetramers). Given that all the synthetic oscillator elements are controlled by the same promoter ($P_{lac/ara}$) K, n, p and γ are the same for both species. A cartoon depicting the model interactions is shown in Figure 12. These ODEs are part of the coupled oscillator model (see Equation (1)a-b).

This system presents a limit cycle for the parameter values shown in Table 1. Note that we assume a non-zero basal production rate because the limit cycle disappears when $\alpha_1 = 0$. In this regard, experiments show that when the synthetic oscillator is not induced, part of the population turns the reporter's expression on, thus demonstrating that that the hybrid promoter $P_{lac/ara}$ is leaky.

The degradation rate of R (δ_2) is assumed to be one order of magnitude smaller than the one of A (δ_1) which can be explained as follows. In the experimental implementation of the oscillator, AraC and LacI are marked with a *ssrA* degradation tag. This tag is recognized by ClpXP, a proteolytic complex composed by ClpX (responsible for unfolding the protein to be degraded) and ClpP (a peptidase)[23]. This tag is also recognized by ClpAP, which analogously to ClpPX is composed by a chaperon (ClpA) and also by the ClpP peptidase[24]. When ClpAP finds an homodimer (which happens when the two protomers -the subunits that constitute an oligomeric protein- have the *ssrA* degradation tag, as it is our case) the most probable scenario is that ClpAP degrades the two subunits at the same time[24]. It is also probable that ClpXP behaves in the same way. However, there is no evi-

dence in the literature that ClpAP and/or ClpXP may degrade a whole tetrameric complex at once. Studies measuring the size of the pore that allows the substrate to reach the active site of ClpP show that this pore would be big enough to simultaneously accommodate between two and three polypeptidic chains[25]. In addition, kinetic experiments with ClpXP machinery indicate that the denaturalization process determines the degradation rate[26]. Hence, it seems reasonable that LacI tetramers (R) degrade more slowly than AraC dimers (A).

Let us illustrate this considering a pool of a protein that assembles in "homo-tetramers". If we denote by D the dimeric conformation and by T the tetrameric form, assuming degradation only occurs enzimatically we have:

$$\frac{dD}{dt} = -k_+ D^2 + \delta_T CT - \delta_D CD$$

$$\frac{dT}{dt} = k_+ D^2 - \delta_T CT$$

where C corresponds to the protease concentration. If we assume that D is in quasi-steady state, we obtain

$$\frac{dT}{dt} = \frac{(\delta_D C)^2}{2k_+} - \frac{\delta_D C}{2k_+}\sqrt{(\delta_D C)^2 + 4k_+\delta_T CT}$$

Given the assumption in k_+, from the previous expression we have that T degrades as $\sim T^{1/2}$. Since in the model Equation (4) we consider only linear degradations, we take this fact into account by assuming a smaller degradation rate for R (LacI tetramers) compared to A degradation rate (AraC dimers).

The Hill coefficients in the synthetic oscillator model, defined by parameters n and p are both equal to 2 and account for changes in DNA conformation. Regarding n, regulation of P_{ara} by AraC is implemented in a positive form (in the presence of arabinose) and in a negative one (in the absence of arabinose) involving DNA looping[27]. Regarding p, the repression of P_{lac} also relies in a DNA looping conformation effect[28].

Acknowledgments

The authors would like to acknowledge Dr. Elena Abad for the Kullback-Leibler divergence computation. This work was supported by the Ministerio de Economia y Competividad and FEDER (Spain, project FIS2012-37655-C02-01), and by AGAUR (project 2012SGR0974). JGO also acknowledges support from the ICREA Academia programme.

Table 1 Parameter values for the coupled oscillator model

Par.	Value	Units	Description
α_1	5.1	nM s^{-1}	A basal production rate
α_2	0.75	nM s^{-1}	R basal production rate
α_3	0.5	nM s^{-1}	B basal production rate
β_1	225	nM s^{-1}	A maximum activated production rate
β_2	30	nM s^{-1}	R maximum activated production rate
β_3	10	nM s^{-1}	B maximum activated production rate
δ_1	0.01158	s^{-1}	A degradation rate
δ_2	0.001158	s^{-1}	R degradation rate
δ_3	0.00025	s^{-1}	B degradation rate
γ	2	-	Ratio of activation to inhibition threshold
K	5000	nM	Concentration of A for half-maximal activation
n	2	-	Activation cooperativity
p	2	-	Inhibition cooperativity
L_0	0.5	a.u.	Initial cell length (when cell is born)
τ	30	min	Characteristic time of the cell growth integrate & fire model
K_I	100	nM	Concentration of B for half-maximal back-coupling
ε	0.75	-	Replication threshold
D_{th}	$2L_0$	a.u.	Division threshold

References

1 B. Novák and J. J. Tyson, *Nature reviews. Molecular cell biology*, 2008, **9**, 981–91.

2 T. Mori, B. Binder and C. H. Johnson, *Proceedings of the National Academy of Sciences of the United States of America*, 1996, **93**, 10183–10188.

3 Q. Yang, B. F. Pando, G. Dong, S. S. Golden and A. van Oudenaarden, *Science*, 2010, **327**, 1522–1526.

4 M. P. Dekens, C. Santoriello, D. Vallone, G. Grassi, D. Whitmore and N. S. Foulkes, *Current Biology*, 2003, **13**, 2051–2057.

5 M. G. Salter, K. A. Franklin and G. C. Whitelam, *Nature*, 2003, **426**, 680–683.

6 E. Nagoshi, C. Saini, C. Bauer, T. Laroche, F. Naef and U. Schibler, *Cell*, 2004, **119**, 693–705.

7 T. Matsuo, S. Yamaguchi, S. Mitsui, A. Emi, F. Shimoda and H. Okamura, *Science*, 2003, **302**, 255–259.

8 C. Gérard and A. Goldbeter, *PLoS computational biology*, 2012, **8**, e1002516.

9 A. Pikovsky, M. Rosenblum and J. Kurths, *Synchronization: a universal concept in nonlinear sciences*, Cambridge University Press, 2003.

10 K. Kaasik and C. C. Lee, *Nature*, 2004, **430**, 467–471.

11 C. Feillet, P. Krusche, F. Tamanini, R. C. Janssens, M. J. Downey, P. Martin, M. Teboul, S. Saito, F. a. Lévi, T. Bretschneider, G. T. J. van der Horst, F. Delaunay and D. a. Rand, *Proceedings of the National Academy of Sciences of the United States of America*, 2014, **111**, 9828–9833.

12 M. G. Rosenblum, A. S. Pikovsky and J. Kurths, *Physical Review Letters*, 1996, **76**, 1804.

13 J. D. Wang and P. A. Levin, *Nature Reviews Microbiology*, 2009,

7, 822–827.
14 W. D. Donachie and G. W. Blakely, *Current opinion in microbiology*, 2003, **6**, 146–150.
15 T. Katayama, S. Ozaki, K. Keyamura and K. Fujimitsu, *Nature Reviews Microbiology*, 2010, **8**, 163–170.
16 J. E. Camara, A. M. Breier, T. Brendler, S. Austin, N. R. Cozzarelli and E. Crooke, *EMBO reports*, 2005, **6**, 736–741.
17 J. M. Kaguni, *Annu. Rev. Microbiol.*, 2006, **60**, 351–371.
18 P. S. Swain, M. B. Elowitz and E. D. Siggia, *Proceedings of the National Academy of Sciences*, 2002, **99**, 12795–12800.
19 J. Stricker, S. Cookson, M. R. Bennett, W. H. Mather, L. S. Tsimring and J. Hasty, *Nature*, 2008, **456**, 516–519.
20 P. Rué and J. Garcia-Ojalvo, *Mathematical Biosciences*, 2011, **231**, 90–97.
21 B. P. Tu, A. Kudlicki, M. Rowicka and S. L. McKnight, *Science*, 2005, **310**, 1152–8.
22 J. Sambrook, E. F. Fritsch, T. Maniatis *et al.*, *Molecular cloning*, Cold spring harbor laboratory press New York, 1989.
23 T. A. Baker and R. T. Sauer, *Biochimica et Biophysica Acta (BBA) - Molecular Cell Research*, 2012, **1823**, 15–28.
24 S. Sharma, J. R. Hoskins and S. Wickner, *Journal of Biological Chemistry*, 2005, **280**, 5449–5455.
25 R. E. Burton, S. M. Siddiqui, Y. I. Kim, T. A. Backer and R. T. Sauer, *EMBO J*, 2001, **20**, 3092–3100.
26 Y.-I. Kim, R. E. Burton, B. M. Burton, R. T. Sauer and T. A. Baker, *Molecular cell*, 2000, **5**, 639–648.
27 R. B. Lobell and R. F. Schleif, *Science*, 1990, **250**, 528–532.
28 M. Lewis, G. Chang, N. C. Horton, M. A. Kercher, H. C. Pace, M. A. Schumacher, R. G. Brennan and P. Lu, *Science*, 1996, **271**, 1247–1254.